HHS Public Access

Author manuscript

Neuron. Author manuscript; available in PMC 2016 July 01.

Published in final edited form as:

Neuron. 2015 July 1; 87(1): 193–207. doi:10.1016/j.neuron.2015.06.019.

An interglomerular circuit gates glomerular output and implements gain control in the mouse olfactory bulb

Arkarup Banerjee[1,2,#], **Fred Marbach**[1,2,#], **Francesca Anselmi**[1], **Matthew S. Koh**[1,2], **Martin B. Davis**[1], **Pedro Garcia da Silva**[1,3], **Kristen Delevich**[1,2], **Hassana K. Oyibo**[1,2], **Priyanka Gupta**[1,4], **Bo Li**[1,2], and **Dinu F. Albeanu**[1,2,*]

[1]Cold Spring Harbor Laboratory, Cold Spring Harbor, NY-11724, USA

[2]Watson School of Biological Sciences, Cold Spring Harbor, NY-11724, USA

[3]Champalimaud Neuroscience Programme, Lisbon-1400-038, Portugal

[4]National Centre for Biological Sciences, Tata Institute of Fundamental Research, Bangalore-560065, India

Summary

Odors elicit distributed activation of glomeruli in the olfactory bulb (OB). Crosstalk between co-active glomeruli has been proposed to perform a variety of computations, facilitating efficient extraction of sensory information by the cortex. Dopaminergic/GABAergic cells in the OB, which can be identified by their expression of the dopamine transporter (DAT), provide the earliest opportunity for such crosstalk. Here we show in mice that DAT+ cells carry concentration dependent odor signals and broadcast focal glomerular inputs throughout the OB to cause suppression of mitral/tufted (M/T) cell firing, an effect that is mediated by the external tufted (ET) cells coupled to DAT+ cells via chemical and electrical synapses. We find that DAT+ cells implement gain control and decorrelate odor representations in the M/T cell population. Our results further indicate that ET cells are gatekeepers of glomerular output and prime determinants of M/T responsiveness.

Introduction

Variation in stimulus intensity far surpasses the output range (firing rate) of individual neurons. To encode stimuli across a wide intensity range (Vickers, 2000), sensory systems employ gain control mechanisms, trading-off sensitivity and resolution to regulate their output in accordance with the expected variation in inputs. The quest to find circuit motifs that mediate gain control has driven a large body of research in various sensory systems,

*Correspondence to: albeanu@cshl.edu.
#Equal contribution.

Author Contributions

A.B., F.M. and D.F.A. conceptualized the study. A.B., F.M., P.G., F.A., M.K., B.L. and D.F.A. contributed to the practical design of experiments and analysis. A.B, F.M., P.G.D.S. and D.F.A. performed *in vivo* OB imaging. A.B and F.M. *in vivo* recordings, M.B.D., A.B. and F.M. viral injections and immunohistochemistry, F.A., M.K. and K.D. patching experiments. P.G. implemented hardware instrumentation and acquisition software for *in vivo* recordings. H.K.O. made the PRV-Cre virus. A.B., F.M., P.G. and D.F.A. wrote the manuscript.

including olfaction (Carandini and Heeger, 1994, 2012; Nikolaev et al., 2013; Ohshiro et al., 2011; Olsen et al., 2010; Robinson and McAlpine, 2009).

Odors are detected in the nasal epithelium by olfactory sensory neurons (OSNs) that project to the olfactory bulb (OB), forming a precise layout of distinct input nodes called glomeruli (Mombaerts, 2006; Shepherd, 1972; Soucy et al., 2009). Each glomerulus receives input from OSNs expressing a given receptor type, out of a repertoire of ~1,100 in the mouse (Buck and Axel, 1991; Mombaerts et al., 1996). A given odor activates a select combination of odorant receptors, triggering activity of multiple glomeruli across the surface of the bulb. Individual M/T cells integrate signals across several co-active glomeruli via interneurons in the glomerular, external plexiform (EPL) and granule cell layers. Despite the diverse interneuron populations in the mammalian OB, surprisingly little is known about their influence on M/T cell dynamics *in vivo*.

Increasing odor concentration not only results in increased response amplitudes of individual glomeruli, but also in the activation/suppression of new glomeruli (Bozza et al., 2004; Meister and Bonhoeffer, 2001; Spors et al., 2006). Therefore gain control mechanisms in the early olfactory circuit are needed to compress the large variation and diversity of glomerular inputs to match the constant dynamic range of individual OB output neurons (M/T cells). Given the spatially distributed nature of odor inputs, bulb micro-circuits need to mediate crosstalk across co-active glomeruli to perform computations such as intensity normalization and population decorrelation (Spors et al., 2012; Wilson, 2013; Wilson and Mainen, 2006). Recently, in the fly and zebra fish olfactory systems, lateral interactions across glomeruli have been shown to implement gain control, and help equalize the population activity of projection neurons (Huang et al., 2010; Olsen and Wilson, 2008; Yaksi and Wilson, 2010; Zhu et al., 2013).

In mammals, a class of dopaminergic/GABAergic interneurons, often referred to as short axon (SA) cells, offers the first opportunity for crosstalk between neighboring, as well as distant glomeruli (Aungst et al., 2003). They receive feed-forward excitatory inputs within individual glomeruli from both excitatory local interneurons (external tufted cells, ET) and OSNs (Aungst et al., 2003). Contrary to their name, SA cells are unique in their ability to extend far-reaching processes, targeting ET cells associated with nearby as well as distant glomeruli located up to 1.5 mm away (~25 glomerular diameters) (Aungst et al., 2003; Kiyokage et al., 2010; Kosaka and Kosaka, 2011; Pinching and Powell, 1971).

Recent *in vitro* studies have shown that SA action on ET cells results in GABAergic hyperpolarization followed by dopamine-mediated (D1) depolarization (Liu et al., 2013; Whitesell et al., 2013). However, the relative excitation versus inhibition conveyed to an M/T cell upon SA activation depends on the interplay between OSN input and the antagonistic action of other excitatory and inhibitory interneurons (ET and PG cells). Therefore, the net effect of SA action on the M/T output in the intact brain cannot easily be extrapolated from *in vitro* experiments.

We genetically targeted dopaminergic/GABAergic (DAT+) interneurons in the glomerular layer of the OB. These cells match the known characteristics of SA cells (Aungst et al.,

2003; Borisovska et al., 2013; Chand et al., 2015; Kiyokage et al., 2010; Kosaka and Kosaka, 2011; Liu et al., 2013; Tatti et al., 2014; Wachowiak et al., 2013; Whitesell et al., 2013). We asked two questions in this study. First, what is the nature of the signals carried by the DAT+ cells? Second, what is the impact of interglomerular crosstalk mediated by DAT+ cells on the activity of M/T cells? We find that odor responses of DAT+ cells scale with concentration, thereby implementing gain control and decorrelating odor representations in M/T cells. Mechanistically, our results indicate that ET cells are gatekeepers of the glomerular output and prime determinants of M/T cell activity.

Results

Genetic targeting of dopaminergic/GABAergic cells in the OB using DAT-Cre mice

We used genetically engineered mice (DAT-Cre) that express Cre recombinase under the control of the dopamine transporter (DAT) promoter (Zhuang et al., 2005) to target expression of a genetically encoded calcium indicator (GCaMP3.0), or optogenetic modulators (channelrhodopsin2, ChR2, and halorhodopsin, NpHR3.0) to dopaminergic cells in the OB. DAT-Cre mice were either crossed to Cre-dependent mouse lines to specifically express tdTomato (Ai9)/ChR2 (Ai32)/GCaMP3.0 (Ai38) or injected with adeno-associated viruses (AAV) carrying a FLEXed transgene.

The targeted DAT+ cells were restricted to the glomerular layer (Figure 1A), consistent with previous studies (Kiyokage et al., 2010; Kosaka and Kosaka, 2011; Liu et al., 2013; Whitesell et al., 2013). Focal injection of AAV2.9-EF1a-DIO-ChR2-EYFP in DAT-Cre mice labeled somata near the injection site, as well as processes of variable length extending up to ~1.3 mm away (n = 2 bulbs, Figure S1A, Kiyokage et al., 2010; Kosaka and Kosaka, 2011). Dual immunolabeling in OB slices of DAT-Cre x Ai32 mice showed that 85% of EYFP expressing neurons were TH+. Further, 96% of all TH+ neurons were also GAD67+ (Figure 1B, Kiyokage et al., 2010; Kosaka and Kosaka, 2011). Similarly, in DAT-Cre mice injected with AAV2.9-EF1a-DIO-ChR2-EYFP, we observed 91% overlap between EYFP+ and TH+ neurons (Figure S1B), corroborating the above results. Consistent with previous reports, we did not find significant overlap (< 6%) between DAT+ cells and VGlut2+ (glutamatergic) interneurons by comparing the ChR2-YFP and anti-vGlut2 fluorescence signals (Figure S1C–D, Ohmomo et al., 2009).

Taken together, we find that the DAT+ cells are Dopaminergic and GABAergic, are localized in the glomerular layer and extend processes of variable length spanning distances of up to ~20 glomerular diameters. These characteristics have been ascribed to (SA) cells, an unfortunate misnomer. To avoid confusion, we will refer to the targeted cells as DAT+ cells throughout this manuscript.

DAT+ cells re-distribute glomerular signals throughout the bulb via long-range processes

As a first step towards understanding the functional role of DAT+ cells, we characterized their responses to a diverse panel of odors (Supplemental table 1) and wide range of concentrations (Figure S1I–J) using widefield imaging of GCaMP3.0 signals in anesthetized mice. Individual odors elicited distinct glomerular activity patterns, along with a broad,

lower amplitude signal, which was present irrespective of the identity of the odor (Figure 1C–F and S2A–B, Supplemental movies 1–2). This broad representation of odors by DAT+ cells was in stark contrast to the discrete and sparse odor maps observed in the same animal via intrinsic optical imaging (IOI), a reliable signature of presynaptic glomerular activity (Figure 1C and S2B-i, Gurden et al., 2006; Soucy et al., 2009). The widespread nature of odor responses in DAT+ cells was also reflected in the strong overlap between odor response spectra of different regions of interest (ROIs) on the bulb surface (Figure 1E). Consequently, responses of any two ROIs chosen randomly or using glomerular outlines identified via IOI were highly similar (Figure 1F). We verified that the broad spatial extent was not due to light scattering by imaging OMP-SynaptopHluorin mice (Figure 1I and S2, Supplemental notes, Bozza et al., 2004). We found that these broad responses were also present in TH-Cre mice (Figure S2J–L, but see Wachowiak et al., 2013, Supplemental notes).

We hypothesized that the widespread response results from activation of the long-range processes of DAT+ cells associated with only a few odor-activated glomeruli. Two-photon imaging supported this hypothesis: for any given odor, we observed odor-specific, focal activation of DAT+ cell bodies associated with only a few select glomeruli (Figure 2A–D). The odor response spectra of individual DAT+ cell bodies were sparse and highly correlated for cells located around the boundaries of the same glomerulus, as compared to randomly chosen DAT+ cell pairs (Figure 2D–E and S2B-iii). Widefield imaging of neuropil responses far from the injection site revealed diffuse signals even though individual neuropil responses were sparse and odor-specific, similar to DAT+ cell bodies (Figure S3, Supplemental notes). We conclude that calcium responses from DAT+ cell neuropil underlie the diffuse component of the widefield signal.

Odor responses of DAT+ cells increase monotonically with concentration

With increasing odor concentration, widefield responses increased in amplitude and spatial spread (Figure 1G–I, Supplemental movies 1–2). In contrast, the glomerular IOI and SpH signals remained focal, even when more glomeruli were recruited at higher concentration (Figure 1G, *bottom* and S2C–F).

We also monitored responses of individual DAT+ cell bodies across odor concentration with two-photon imaging (Figure 2F–I). Population analysis of calcium responses pooled either across glomeruli or individual cell bodies, showed a monotonic increase in response amplitude with odor concentration (Figure 2H–I). Taken together, these results suggest that DAT+ cells broadcast signals throughout the glomerular layer via their far-reaching neuropil, thereby spatially re-distributing glomerular inputs in a concentration dependent manner.

Optogenetic activation of DAT+ cells suppresses spontaneous and odor-evoked firing of M/T cells

How does the widespread activity of DAT+ cells influence M/T output? We recorded the firing of individual M/T cells using tetrodes, while optogenetically stimulating ChR2-expressing DAT+ cells throughout the bulb surface via digital micro-mirror device (DMD)

based patterned illumination (Figure 3A, Dhawale et al., 2010). Systematic mapping of the bulb surface with blue light spots showed long-distance inhibition of the spontaneous firing of M/T units, consistent with a broadcasting role of DAT+ cells (Figure 3B). Decreasing light intensity systematically reduced the overall inhibitory strength, while still evoking significant inhibition upon photostimulation as far as 1.5 mm from the recording site (Figure 3B–C and S4A–B). The observed long-range M/T inhibition may either result from stimulation of distal DAT+ cell bodies that project to the recorded neuron, or from antidromic activation of nearby cell bodies upon stimulation of distant axons (Figure 3A, *top*). However, both these scenarios support the long-range inhibition of M/T cells by DAT+ cells. Full-field stimulation of ChR2-expressing DAT+ cells also reliably inhibited M/T odor responses. Increasing light intensity resulted in greater suppression of M/T responses, although individual M/T cell inhibition curves differed even for simultaneously recorded cells (Figure 3D–E). Furthermore, stimulation with arbitrary combinations of glomerulus-sized spots also significantly inhibited odor responses of M/T cells (Figure 3F–G and S4E–F, see Methods). A previous *in-vitro* study reported that activating SA cells briefly (20 ms) elicited a bi-phasic excitation-inhibition sequence in ET cells, potentially patterning M/T cell activity (Liu et al., 2013). However, brief light stimulation (10 to 50 ms) of DAT+ cells *in vivo* resulted in robust suppression of spontaneous activity of M/T cells without any apparent increase in firing rate (Figure S4D). Together these results suggest a long-range inhibitory drive from DAT+ cells to M/T cells.

Optogenetic and pharmacogenetic silencing of DAT+ cells suppresses M/T firing

ChR2 stimulation provided *in vivo* evidence for the inhibitory action of DAT+ cells. To isolate their contribution to the odor-evoked M/T output, we performed loss-of-function manipulations. We expressed NpHR3.0 in DAT+ cells throughout the dorsal bulb surface while monitoring M/T cell activity with tetrodes. We quantified the light-induced change in firing rate (FR) using a change index (CI) defined as $[(FR_{odor} - FR_{odor+light})/(FR_{odor} + FR_{odor+light})]$. Reduced M/T firing upon photostimulation results in $CI > 0$, indicating an excitatory action of DAT+ cells, whereas increase in firing rate results in $CI < 0$, indicating inhibitory action.

Surprisingly, optogenetic silencing of DAT+ cells by full-field illumination suppressed M/T firing, resulting in positive CIs across all odor concentrations indicating an excitatory drive (Figure 4A–C and S5A). Even for the strongest response/stimulus pairs where DAT+ cells were expected to be strongly inhibitory, the average CI was not significantly smaller than zero (Figure 4C). To investigate the spatial extent of M/T cell suppression, we mapped the bulb surface with yellow light spots (Figure 4D-i). Light-induced suppression of spontaneous M/T firing decreased with distance from the recording site. We observed inhibitory ‘coldspots’ (Figure S5B) for co-recorded M/T units that were often non-overlapping, in contrast with the broad extent of the inhibitory effect observed in ChR2 experiments. Light stimulation in wild-type mice under identical conditions did not significantly alter M/T firing (Figure S7A).

To confirm the unexpected suppression of M/T cell activity upon optogenetic silencing of DAT+ cells via an alternative approach, we used a viral strategy (Oyibo et al., 2014) to

simultaneously label M/T cells with GCaMP3.0 and DAT+ cells with both GCaMP3.0 and DREADDi (Figure S5C, designer receptors exclusively activated by designer drugs, Ferguson et al., 2011). Within this framework, intra-peritoneal injection of the DREADDi ligand, clozapine-N-oxide (CNO), suppresses the activity of cells expressing DREADDi by opening hyperpolarizing K+ channels. We verified that injection of CNO significantly decreased odor responses of DAT+ cells co-expressing DREADDi and GCaMP3.0, and had no significant effect on M/T odor responses in DAT-negative mice (Figure S5D–E and S7B).

We monitored the responses of M/T cells to odors across a range of concentrations (~ 3 orders of magnitude), before and after silencing DAT+ cells with DREADDi. M/T odor responses were characteristically different from responses of DAT+ cells, with diverse concentration response curves and temporal dynamics (Harrison and Scott, 1986; Meredith, 1986; Stopfer et al., 2003). Silencing DAT+ cells reduced both excitatory and inhibitory odor responses of M/T cells, resulting in decreased variance of the M/T odor response distribution (Figure S5F–H). Thus, both NpHR3.0 and DREADDi manipulations of DAT+ cells decreased odor responsiveness of M/T cells.

Chemical and Electrical synapses between DAT+ cells and ET cells modulate M/T firing

Surprisingly, both our gain and loss-of-function experiments resulted in the suppression of M/T activity. Electrical coupling between heterogeneous cell types has been observed in the early sensory systems (Apostolides and Trussell, 2013; Farrow et al., 2013; Huang et al., 2010; Yaksi and Wilson, 2010; Zhu et al., 2013). DREADDi or NpHR3.0 mediated silencing of DAT+ cells could in principle lead to hyperpolarizing current flow due to electrical coupling, thereby suppressing M/T cells. This scenario is consistent with the suppression of M/T cell responses and the observed local ‘cold spots’ revealed by NpHR3.0 experiments (Figure 4 and S5).

We thus investigated the possibility of electrical coupling between DAT+ cells and M/T cells. Consistent with this idea, the observed M/T suppression upon photo-stimulating ChR2-expressing DAT+ cells reliably turned into excitation upon topical application of glutamatergic and GABAergic antagonists (Figure 5 and S6A). Application of D1 and D2 receptor antagonists in addition to the glutamatergic and GABAergic antagonists resulted in the same effect (Figure S6C). Similar results were observed with topical application of cadmium chloride, which blocks calcium dependent neurotransmitter release (Figure 5D and S6B). However, even though spontaneous activity of M/T units was reliably blocked, odor-evoked responses were not completely abolished upon drug application (Figure S6D). Despite this caveat, electrical coupling remains the most parsimonious explanation of the observed effect.

To investigate the interaction between DAT+ and M/T cells under more controlled experimental conditions, we performed *in vitro* whole cell recordings from mitral cells while photoactivating DAT+. Consistent with a recent study (Whitesell et al., 2013), we found no direct synaptic inhibition onto mitral cells. Surprisingly, we did not find evidence for electrical coupling either (Figure S7 and S8, Supplemental notes).

Previous *in vitro* studies have reported that ET cells are a major source of excitatory input to M/T cells (Gire et al., 2012; De Saint Jan et al., 2009) and also the principal synaptic target of SA cells (Liu et al., 2013; Whitesell et al., 2013). We thus tested the possibility of electrical coupling between DAT+ cells and ET cells. We performed whole cell recordings from ET cells in acute bulb slices (Figure 6A), while stimulating DAT+ cells expressing ChR2 via full-field blue light stimulation. We observed a robust light-evoked outward current at −30 mV holding potential in ET cells, which switched sign to an inward current at more negative potentials (<−60 mV), indicating GABAergic origin, consistent with a recent report (Figure 6B, Whitesell et al., 2013). Furthermore, application of synaptic blockers completely blocked spontaneous EPSCs and abolished the outward current (Figure 6B–C). However, at hyperpolarized membrane potentials (−90 mV), synaptic blockers application altered a fast component of the light-evoked inward current, unmasking a slow rising component (Figure 6B–C), suggesting electrical coupling. We did not observe any appreciable inward current after synaptic block at −30 mV holding potential. This may be because of a residual synaptic outward current due to incomplete drug action masking the much smaller inward gap-junction current (Figure 6B-ii, top).

To avoid indirect and residual synaptic effects, we resorted to hyperpolarizing DAT+ cells using NpHR3.0 while recording from ET cells. Upon photostimulation, we observed a slow-rising outward current in ET cells (−70 mV holding potential, Figure 6D) as well as hyperpolarization in current clamp recordings (Figure S8E). In an independent set of experiments, application of synaptic blockers abolished the spontaneous synaptic events in ET cells, but did not alter the yellow-light induced outward current (Figure 6D–E). Together, these results strongly support the existence of gap junctions between DAT+ cells and ET cells in addition to synaptic coupling.

Gain control and decorrelation of mitral cell odor representations by DAT+ cells

Gap-junction coupling between DAT+ and ET cells makes it difficult to interpret the results of silencing experiments that rely on hyperpolarization (NpHR3.0 and DREADDi) of DAT+ cells. NpHR3.0 stimulation not only silences the odor-activated DAT+ cells, but also induces hyperpolarization of ET cells (Figure S8E), a major driving force for M/T firing. This may explain the net decrease in M/T responsiveness, instead of the expected disinhibition of M/T firing (Figure 4 and S5). Therefore, we pursued an alternative strategy (Azim et al., 2014) to specifically ablate DAT+ cells in the OB. We expressed Cre-dependent diptheria toxin receptor (AAV-FLEX-DTR-GFP) in DAT+ cells. Three weeks post viral infection, we administered diphteria toxin (DT) intraperitonealy (see Methods), and after one week assessed the effects of this manipulation on DAT+ cell by anti-TH immunohistochemistry in OB slices. On average, the density of TH+ neurons was drastically reduced: < 10% TH+ cells on the dorsal OB surface compared to the ventral aspect of the bulb within the same slices (Figure 7A).

We combined DTR/DT induced ablation of DAT+ cells in the OB with simultaneous optical monitoring of odor responses in mitral cells in DAT-Cre x Thy1 GCaMP3.0 mice, which sparsely express GCaMP3.0 in M/T cells (Chen et al., 2012). We used two-photon imaging to chronically monitor mitral cell odor responses to the same stimuli used previously, either

in the presence (control condition) or absence of DAT+ cells (post-ablation, +DT condition) across different fields of view (FOV), in the same animal or across individuals. As expected, in the control condition, mitral cells (MCs) showed a wide variety of concentration response curves and temporal dynamics (n = 168 cells, 7 FOVs, 7 mice, Figure 7B–F). Ablation of DAT+ cells significantly altered the concentration dependence of MC odor responses: most MC concentration response curves scaled monotonically with stimulus intensity (Figure 7B–C) and the mean MC odor response amplitude was substantially higher (n = 150 cells, 7 FOVs, 3 mice, Figure 7D). Ablation of DAT+ cells also altered the temporal dynamics of MC responses, substantially reducing both the mean and the variance of onset latency in the odor responses (Figure 7C-i) Furthermore, the cumulative distribution of MC response strengths across concentrations showed significantly larger variance in the absence of DAT+ cells (Figure 7E, two-sample F test, $p < 0.001$). Therefore, the concentration dependent inhibition of MCs by DAT+ cells stabilizes not only their mean response amplitude, but also the entire distribution over a wide range of odor concentrations

To determine whether DAT+ cells implement gain control of MC odor responses, we quantified the slope of the mean MC population response for each FOV as a function of concentration. We observed a substantial rightward shift in the distribution of MC population response slopes post-ablation of DAT+ cells (Figure 7F, n = 35, 7 FOV for 5 odors, 2 sample t-test, $p < 0.01$). In addition, for each odor concentration, we observed denser activation of imaged MCs as quantified by a decrease in the population sparseness (Figure 7G, see Methods). Computationally, sparsening of neuronal activity has been proposed as an efficient mechanism for decorrelating different inputs. Indeed, the pairwise odor similarity (defined as the correlation coefficient between the neuronal response spectra of odor pairs, pooled across all cells, see Methods) was significantly higher post-ablation of DAT+ cells compared to control (Figure 7H).

Taken together, our results indicate that DAT+ cells implement gain control by suppressing MC responses with increasing odor concentration, thereby decorrelating MC representations across odors and stimulus intensities.

Discussion

In this study, we genetically targeted dopaminergic/GABAergic (DAT+) interneurons in the mouse OB (Figure 1). These cells reside in the glomerular layer of the OB and match the known characteristics of short axon cells. DAT+ cells re-distribute focal odor inputs and broadcast long-range signals across the glomerular layer. The spatial spread and amplitude of these responses increase with odor concentration (Figure 1–2). DAT+ cells convey local and far-reaching synaptic inhibition to M/T cells indirectly (Figure 3). We find that DAT+ cells modulate the onset dynamics of mitral cells, decrease the gain of M/T population responses and decorrelate odor representations via concentration dependent inhibition (Figure 7). Additionally, we provide evidence for electrical coupling between ET and DAT+ cells (Figure 4, 5 and 6). Our results indicate that ET cells are gatekeepers of the glomerulus output and that synaptic and electrical interactions between DAT+ cells and ET cells tightly regulate the responsiveness of M/T cells to odors (Figure 8).

Long range crosstalk in the glomerular layer

Odors activate distinct patterns of glomeruli that are non-topographically distributed across the OB surface. Interglomerular crosstalk has been proposed to be implemented by a rich diversity of interneurons (PG, PV+ and granule cells), which operate at different stages and spatial scales in the circuit (Kato et al., 2013; Miyamichi et al., 2013; Wilson and Mainen, 2006). Recently PV+ cells in the EPL have been shown to sample inputs from M/T cell dendrites across ~250 μm and, in turn, provide feedback inhibition to the M/T cells within the same area of reach (Kato et al., 2013; Miyamichi et al., 2013). In contrast, interneurons in the glomerular layer such as DAT+ cells receive inputs directly or indirectly from OSNs, and are therefore poised to mediate feedforward inhibition of mitral cells (Linster and Cleland, 2009). DAT+ cells offer the first opportunity for crosstalk between distant co-active glomeruli because of their unique ability to transmit long-range signals (~1.5 mm).

Indeed, we found that the ensemble response of DAT+ cells was odor-indiscriminate and highly correlated across the bulb surface (Figure 1, S2 and Supplemental movies 1–3). Individual DAT+ cells responded to odors as sparsely as individual glomeruli (Figure S2B). Thus, the high spatial correlation is likely due to the overlapping neuropil from DAT+ cells affiliated with different glomeruli (Figure 2, S2 and S3). This mixing of glomerular inputs by long-range neuropil of DAT+ cells may enable M/T cells to pool inputs from numerous co-active, but spatially distributed glomeruli. Consistent with this idea, we found that the firing of M/T cells was significantly suppressed upon stimulation of DAT+ cells across a large area on the OB surface (Figure 3).

Thus, from a very early stage in olfactory processing, the output of a glomerulus is not only determined by direct OSN input, but also by signals originating from other glomeruli, similar to reports in *Drosophila* and zebrafish olfactory systems (Huang et al., 2010; Olsen and Wilson, 2008; Olsen et al., 2010; Yaksi and Wilson, 2010; Zhu et al., 2013).

Gain control and decorrelation of the OB outputs by DAT+ cells

DAT+ cells receive feed-forward odor inputs and their activity and spatial spread scales with increasing odor concentration (Figure 1 and 2). What might be the functional relevance of this concentration dependent and widespread inhibition mediated by DAT+ cells? Individual M/T cells show a wide variety of concentration response curves (Figure 7C and S5G). However, the average population response strength grows modestly with concentration. Ablating DAT+ cells resulted in a significantly steeper concentration response curves for the population, and for individual M/T cells. Further, population responses of M/T cells became denser and more correlated across odors in the absence of DAT+ cells (Figure 7). Our results indicate that DAT+ cells normalize glomerular output through concentration dependent inhibition, thereby increasing the input dynamic range of the M/T cell population. Consistent with this interpretation, concentration dependent gain control by DAT+ cells stabilizes not only the mean response amplitude, but also the variance of the response histogram (Figure 7). Further, DAT+ cells sparsen M/T responses, allowing for decorrelated odor representations. Normalization and decorrelation of population responses in the sensory periphery has been suggested to aid separation of stimuli by subsequent cortical areas in various sensory modalities (Barlow, Horace, 1961; Luo et al., 2010; Olsen et al., 2010;

Vinje and Gallant, 2000). In addition, our results suggest that DAT+ cells are necessary for maintaining the diversity of onset latencies observed in mitral cell odor responses, and thus may also be involved in computations other than gain control.

Mechanistically, dense convergence of sparsely responding DAT+ cells from many glomeruli onto individual ET cells would result in sum total inhibition that is proportional to stimulus strength, and thus normalize glomerular output. The broadly tuned ensemble responses of DAT+ cells in any local region observed in our widefield imaging experiments (Figure 1), as well as the widespread M/T inhibition upon focal activation of DAT+ cells (Figure 3), are consistent with this scenario. Even with sparser connectivity, long-range broadcast of inhibition by DAT+ cells will result in suppression of weakly responding glomeruli, thereby enhancing the contrast of glomerular activity maps. In either connectivity scenario, the action of DAT+ cells would increase the separability of odor representations in the M/T population. Future experiments combining optogenetic activation of DAT+ cells at glomerular resolution, while monitoring M/T or ET cell activity, will allow direct analysis of the spatial extent, density and specificity of functional connectivity in the glomerular network.

A recent computational model posited that SA cells implement global normalization of M/T cell responses (Cleland, 2010). This model proposes that SA-ET-SA interactions constitute a small-world network that integrates excitatory inputs across many glomeruli. Thus, within each glomerulus, PG cells inherit a globally averaged signal from ET cells, and in turn inhibit M/T cells, ultimately leading to decorrelation of odor representations. This model requires the SA cells to be excitatory (Aungst et al 2003). Although our results (Figure 6) rule out the proposed mechanism, the function of DAT+ cells is consistent with this model.

Synaptic and electrical coupling in the glomerular layer

We found that in addition to synaptic inhibition, DAT+ cells may also influence ET cells via gap-junctions (Figure 5 and 6). Multiple aspects of our data suggest the existence of electrical coupling between DAT+ and ET cells. In the presence of synaptic blockers, ChR2 stimulation of DAT+ cells evoked a slow-rising depolarizing current in ET cells (Figure 6B–C). Conversely, NpHR3.0 silencing of DAT+ cells resulted in a slow-rising hyperpolarizing current in ET cells, which persisted even after application of synaptic blockers (Figure 6D–E). NpHR3.0 silencing *in vivo* also resulted in local suppression of M/T responses (Figure 4D), as would be expected by direct hyperpolarization of ET cells via gap-junctions (Figure S8E). Further, DAT+ cell mediated inhibition of M/T cells switched to excitation upon synaptic block (Figure 5 and S6).

What may be the functional implications of the opposing electrical and synaptic interactions between DAT+ and ET cells? Similar architectures of electrically and synaptically coupled interneurons in the fly and fish olfactory systems have been proposed to bi-directionally modulate the firing of projection neurons, by boosting weak odor responses through gap junctions and suppressing strong responses via synaptic inhibition (Huang et al., 2010; Yaksi and Wilson, 2010; Zhu et al., 2013). Electrical coupling between DAT+ and ET cells may also underlie indirect lateral excitation of M/T cells.

The regime in which DAT+ cells could influence ET and M/T cells through gap-junctions is however constrained by the local spatial scale of effective electrical coupling (Figure 4D and S5B) and the consistently dominant influence of synaptic inhibition observed in our experiments. We did not observe an excitatory effect of DAT+ cells on M/T responses upon genetic ablation of DAT+ cells (Figure 7) or even upon weak ChR2 stimulation of DAT+ cells (Figure 3 and S4). The excitatory influence of DAT+ cells may however be effective under weaker stimulus conditions, which fail to trigger spiking in DAT+ cells and consequently synaptic inhibition of ET cells.

Intra-glomerular gap-junctions in the mammalian OB have also been proposed to synchronize firing of M/T, as well as of ET cells within the same glomerulus (Christie et al., 2005; Hayar et al., 2005; Schoppa and Westbrook, 2002). Gap junctions may therefore enable ET cells to recruit strong, synchronous and fast spread of inhibition across the glomerular layer, by activating DAT+ cells within the same glomerulus through both electrical and synaptic mechanisms. The roles played by electrical coupling in sensory circuits are just beginning to be explored. In the retina, the extent and potency of electrical coupling can rapidly expand when light levels change (Bloomfield and Völgyi, 2009), in turn modulating the impact of gap junctions on visual processing. Future studies performed in low stimulus concentration regimes in awake behaving animals will elucidate the full extent of the roles played by electrical coupling between DAT+ and ET cells.

ET cells are the gatekeepers of glomerular output

Recent *in vitro* studies (Gire et al., 2012; De Saint Jan et al., 2009) have proposed that ET cells provide the primary excitatory drive to M/T cells within a glomerulus, in contrast with the canonical direct OSN→M/T flow of excitation. These results have been a matter of debate, as they propose an important reconsideration of the basic logic of the bulb circuitry. Several aspects of our data provide the first *in vivo* evidence for the central role of ET cells in determining mitral cell responsiveness.

Odor-evoked spiking in M/T cells was strongly suppressed upon optogenetic activation of DAT+ cells *in vivo*, despite the apparent lack of direct DAT+ to M/T connections (Figures 3 and S8). Given that ET cells are the principal targets of GABAergic inhibition from DAT+ cells (Figures 6 and S8, Whitesell et al., 2013), our *in vivo* results suggest that the majority of odor input to a glomerulus is relayed to M/T cells through ET cells, and not directly from the OSNs. Furthermore, optogenetic silencing of DAT+ cells hyperpolarized ET cells *in vitro* (Figure S8E) and greatly reduced M/T odor responses *in vivo* (Figure 4). These results suggest that reduced ET excitability significantly attenuates the odor-induced excitatory drive onto M/T cells (Figure 8). We infer that ET cells act as gatekeepers of glomerular output and regulate the excitability of M/T cells *in vivo*. DAT+ cells suitably target this principal node in the glomerulus allowing for crosstalk between co-activated glomeruli and strict control of M/T spiking before the EPL or GC interneuronal networks.

In this study, we have not explored the role of dopamine released by DAT+ cells and in general the implication of dual neurotransmission in olfactory processing. Preliminary results show that blocking D1 receptors decreases M/T firing (*data not shown*), suggesting the existence of a synaptic excitatory role of DAT+ cells. Future studies will help understand

how the interplay between dopaminergic, GABAergic and electrical action of DAT+ cells influences OB output.

Finally, our results emphasize that substantial transformation of odor representations occurs in the input layer of the olfactory bulb. These findings open exciting venues to further elucidate the downstream impact of glomerular layer processing on olfactory computations and behavior.

Experimental Procedures

Animals and surgical methods

All experiments were done in adult mice in accordance with NIH guidelines and CSHL Animal Care and Use Committee. Mice were anesthetized with Ketamine-Xylazine (KX) injections and body temperature was maintained at 37° C. Craniotomy was performed to expose the dorsal OB and covered with a thin layer of 1.2% agarose. For extracellular recordings, dura mater was removed and a pair of tetrodes (octrodes) was inserted. For acute imaging experiments, a glass cover slide was placed to prevent drying and reduce motion artifacts, whereas a glass window (~ 3 mm) was implanted for chronic two-photon imaging. DAT-Cre specific targeting of ChR2, NpHR3.0, GCaMP3.0, DREADDi and DTR was achieved using AAV injections at 2–3 sites in the dorsal OB.

Odor delivery

Odors were delivered using a custom-made odor machine as described previously (Dhawale et al., 2010). Odors were diluted at 1:100 in mineral oil unless specified otherwise. Throughout the manuscript, concentrations of odors are expressed as nominal dilutions in mineral oil (odor-oil volume ratio). Each odor trial was flanked by air periods and inter-trial intervals were 15–60 seconds.

Photostimulation and electrical recordings

Patterned photostimulation of the olfactory bulb using a DLP projector and simultaneous extracellular recordings of M/T cells were performed as described previously (Dhawale et al., 2010). For patch-clamp recordings, signals were recorded with a Multiclamp 700B, low-pass filtered at 10 kHz and digitized at 10 kHz with an analog-to-digital converter Digidata 1440A, using Clampex 10.2 software (Axon Instruments, Molecular Devices). Anatomical location, in-vitro fluorescence, spiking characteristics and morphology visualized by post-hoc dye filling were used to identify the cell-types.

Imaging

LED arrays were used to shine blue light for widefield GCaMP3.0 imaging and far red light (780 nm) for intrinsic optical imaging (IOI). Images were acquired at 25Hz for IOI and 4Hz for widefield GCaMP3.0 imaging with a Vosskühler 1300-QF CCD camera. Two-photon imaging (5Hz) was performed with a custom-built microscope and acquisition software in Labview using a collimated laser beam (930 nm) from a Ti-Sa 80MHz pulsed laser to backfill a 20X 1.0 NA Olympus objective lens.

Pharmacology and Ablation of DAT+ cells

Drug cocktails were superfused over the exposed OB surface 30 minutes prior to the recording and continuously thereafter. For synaptic block experiments, a cocktail of CNQX, APV, BMI or $CdCl_2$ (each at 1mM) was used. In some experiments (Figure S6C) D1 antagonist SKF83566 hydrobromide and D2 antagonist Sulpiride (1mM concentration) were also added to block dopaminergic transmission. For DREADDi inactivation experiments (Figure S5), Clozapine-N-oxide (CNO), diluted in saline to a concentration of 4mg/ml was injected I.P. at a final concentration of 5–10 mg/Kg of body weight. Post-CNO imaging session started 30 minutes after the injection. For genetic ablation of DAT+ cells (Figure 7), DAT-Cre or DAT-Cre X Thy1-GCaMP3.0 mice were injected in the OB with AAV-FLEX-DTR-GFP virus (gift from T Jessell and E. Azim, Columbia University). 2–3 weeks post injection, either saline or 400 ng of diphtheria toxin (DT, Sigma) was administered I.P. Animals were chronically imaged using two-photon microscopy on DAY0 (immediately before injecting DT) and 1–2 weeks (DAYS 7–14) subsequently. In some animals, windows were implanted on DAY 7, 1 week after injection of DT. Data from both conditions were pooled.

Imaging analyses

Response strength was quantified as the normalized change in reflectance (dR/R, IOI) or in fluorescence (dF/F, calcium imaging) averaged across repeats. Regions-of-interest (ROIs) were chosen and response strength was calculated by averaging over all the pixels in each ROI. The spatial spread of odor responses was calculated by determining the fraction of pixels that responded above 2 SD from the baseline average during air period. *Lifetime Sparseness* was calculated using a modified metric (Willmore and Tolhurst, 2001) to quantify the extent to which a given unit is modulated by different stimuli.

$$LS_i = 1 - \frac{\left(\sum_{j=1}^{m} \frac{r_j}{m}\right)^2}{\sum_{j=1}^{m} \frac{r_j{}^2}{m}}$$

i = ROI index for which lifetime sparseness is calculated;

m = *number of odors*

r_j = *response of the ROI to the odor number j*

Similarity—We used as a similarity metric, the uncentered correlation coefficient among their odor response spectra (ORS). Similarity between ROIs A and B:

$$S^{(A,B)} = \frac{\sum_{j=1}^{n} r_j^{(A)} \cdot r_j^{(B)}}{\sqrt{\sum_{j=1}^{n} r_j^{(A)} \cdot r_j^{(A)}} \cdot \sqrt{\sum_{j=1}^{n} r_j^{(B)} \cdot r_j^{(B)}}}$$

r_j = response of ROI to odor j,

n = number of odors.

Population response was calculated as the mean of the response strengths to a given odor either across all the neurons in a given FOV or all the recorded neurons pooled across experiments. For each odor stimulus, the neuronal response spectrum (NRS) was constructed as a vector containing the response strengths of all the recorded mitral cells pooled across FOVs (length = # of cells) and was used to calculate *Population sparseness.* For each stimulus pair, the Pearson correlation coefficient of these NRS was calculated to represent *odor similarity*. All figures denote Mean +− SEM unless explicitly specified.

Electrophysiology analyses

For optogenetic mapping experiments, individual light spots that significantly modulated ('significant spots') the firing rate (FR) of the recorded unit in either direction compared to the 'pre-light' period was assessed using a two-sample t-test ($p < 0.05$). M/T responses were calculated as the mean FR during the 'baseline', 'odor' or 'odor + light' periods across all repeats. For each M/T unit, a significance value (p-value) was calculated for every 'odor' and 'odor + light' pair (two-sample t-test) across the repeats. For ChR2 light-mapping experiments with drugs, we identified spots that significantly modulated the FR upon light stimulation during the drug period, same as above. For each significant spot, the light induced FR change was compared in the control (pre-drug) and drug condition. For a given M/T unit, we calculated the time-course of the light-induced response by computing the mean PSTH across all significant spots.

Supplementary Material

Refer to Web version on PubMed Central for supplementary material.

Acknowledgments

We would like to thank A. Dhawale, G. Otazu, S. Shea, A. Zador and A. Kepecs for valuable scientific discussions and inputs on manuscript preparation, R. Eifert for machine shop assistance, T. Jessel and E. Azim for gift of DTR virus, M. Luo for the gift of DREADD virus and members of the Albeanu laboratory for comments on the manuscript. This study was supported by an NIDCD R01 grant, an EMBO Fellowship, CSHL startup funds, Crick-Clay fellowship and Farish-Gerry fellowship.

References

Apostolides PF, Trussell LO. Regulation of interneuron excitability by gap junction coupling with principal cells. Nat Neurosci. 2013; 16:1764–1772. [PubMed: 24185427]

Aungst JL, Heyward PM, Puche AC, Karnup SV, Hayar A, Szabo G, Shipley MT. Centre-surround inhibition among olfactory bulb glomeruli. Nature. 2003; 426:623–629. [PubMed: 14668854]

Azim E, Jiang J, Alstermark B, Jessell TM. Skilled reaching relies on a V2a propriospinal internal copy circuit. Nature. 2014; 508:357–363. [PubMed: 24487617]

Barlow, Horace. Possible principles underlying the transformation of sensory messages. Rosenblith, WA., editor. MIT Press; Cambridge, MA: 1961.

Bloomfield SA, Völgyi B. The diverse functional roles and regulation of neuronal gap junctions in the retina. Nat Rev Neurosci. 2009; 10:495–506. [PubMed: 19491906]

Borisovska M, Bensen AL, Chong G, Westbrook GL. Distinct modes of dopamine and GABA release in a dual transmitter neuron. J Neurosci. 2013; 33:1790–1796. [PubMed: 23365218]

Bozza T, McGann JP, Mombaerts P, Wachowiak M. In vivo imaging of neuronal activity by targeted expression of a genetically encoded probe in the mouse. Neuron. 2004; 42:9–21. [PubMed: 15066261]

Buck L, Axel R. A novel multigene family may encode odorant receptors: A molecular basis for odor recognition. Cell. 1991; 65:175–187. [PubMed: 1840504]

Carandini M, Heeger DJ. Summation and division by neurons in primate visual cortex. Science. 1994; 264:1333–1336. [PubMed: 8191289]

Carandini M, Heeger DJ. Normalization as a canonical neural computation. Nat Rev Neurosci. 2012; 13:51–62. [PubMed: 22108672]

Chand AN, Galliano E, Chesters RA, Grubb MS. A distinct subtype of dopaminergic interneuron displays inverted structural plasticity at the axon initial segment. J Neurosci. 2015; 35:1573–1590. [PubMed: 25632134]

Chen Q, Cichon J, Wang W, Qiu L, Lee SJR, Campbell NR, Destefino N, Goard MJ, Fu Z, Yasuda R, et al. Imaging neural activity using Thy1-GCaMP transgenic mice. Neuron. 2012; 76:297–308. [PubMed: 23083733]

Christie JM, Bark C, Hormuzdi SG, Helbig I, Monyer H, Westbrook GL. Connexin36 mediates spike synchrony in olfactory bulb glomeruli. Neuron. 2005; 46:761–772. [PubMed: 15924862]

Cleland TA. Early transformations in odor representation. Trends Neurosci. 2010; 33:130–139. [PubMed: 20060600]

Dhawale AK, Hagiwara A, Bhalla US, Murthy VN, Albeanu DF. Non-redundant odor coding by sister mitral cells revealed by light addressable glomeruli in the mouse. Nat Neurosci. 2010; 13:1404–1412. [PubMed: 20953197]

Farrow K, Teixeira M, Szikra T, Viney TJ, Balint K, Yonehara K, Roska B. Ambient illumination toggles a neuronal circuit switch in the retina and visual perception at cone threshold. Neuron. 2013; 78:325–338. [PubMed: 23541902]

Ferguson SM, Eskenazi D, Ishikawa M, Wanat MJ, Phillips PEM, Dong Y, Roth BL, Neumaier JF. Transient neuronal inhibition reveals opposing roles of indirect and direct pathways in sensitization. Nat Neurosci. 2011; 14:22–24. [PubMed: 21131952]

Gire DH, Franks KM, Zak JD, Tanaka KF, Whitesell JD, Mulligan AA, Hen R, Schoppa NE. Mitral cells in the olfactory bulb are mainly excited through a multistep signaling path. J Neurosci. 2012; 32:2964–2975. [PubMed: 22378870]

Gurden H, Uchida N, Mainen ZF. Sensory-evoked intrinsic optical signals in the olfactory bulb are coupled to glutamate release and uptake. Neuron. 2006; 52:335–345. [PubMed: 17046695]

Harrison TA, Scott JW. Olfactory bulb responses to odor stimulation: analysis of response pattern and intensity relationships. J Neurophysiol. 1986; 56:1571–1589. [PubMed: 3806183]

Hayar A, Shipley MT, Ennis M. Olfactory bulb external tufted cells are synchronized by multiple intraglomerular mechanisms. J Neurosci. 2005; 25:8197–8208. [PubMed: 16148227]

Huang J, Zhang W, Qiao W, Hu A, Wang Z. Functional connectivity and selective odor responses of excitatory local interneurons in Drosophila antennal lobe. Neuron. 2010; 67:1021–1033. [PubMed: 20869598]

Kato HK, Gillet SN, Peters AJ, Isaacson JS, Komiyama T. Parvalbumin-expressing interneurons linearly control olfactory bulb output. Neuron. 2013; 80:1218–1231. [PubMed: 24239124]

Kiyokage E, Pan YZ, Shao Z, Kobayashi K, Szabo G, Yanagawa Y, Obata K, Okano H, Toida K, Puche AC, et al. Molecular identity of periglomerular and short axon cells. J Neurosci. 2010; 30:1185–1196. [PubMed: 20089927]

Kosaka T, Kosaka K. “Interneurons” in the olfactory bulb revisited. Neurosci Res. 2011; 69:93–99. [PubMed: 20955739]

Linster C, Cleland TA. Glomerular microcircuits in the olfactory bulb. Neural Netw. 2009; 22:1169–1173. [PubMed: 19646847]

Liu S, Plachez C, Shao Z, Puche A, Shipley MT. Olfactory bulb short axon cell release of GABA and dopamine produces a temporally biphasic inhibition-excitation response in external tufted cells. J Neurosci. 2013; 33:2916–2926. [PubMed: 23407950]

Luo SX, Axel R, Abbott LF. Generating sparse and selective third-order responses in the olfactory system of the fly. Proc Natl Acad Sci USA. 2010; 107:10713–10718. [PubMed: 20498080]

Meister M, Bonhoeffer T. Tuning and topography in an odor map on the rat olfactory bulb. J Neurosci. 2001; 21:1351–1360. [PubMed: 11160406]

Meredith M. Patterned response to odor in mammalian olfactory bulb: the influence of intensity. J Neurophysiol. 1986; 56:572–597. [PubMed: 3537224]

Miyamichi K, Shlomai-Fuchs Y, Shu M, Weissbourd BC, Luo L, Mizrahi A. Dissecting local circuits: parvalbumin interneurons underlie broad feedback control of olfactory bulb output. Neuron. 2013; 80:1232–1245. [PubMed: 24239125]

Mombaerts P. Axonal wiring in the mouse olfactory system. Annu Rev Cell Dev Biol. 2006; 22:713–737. [PubMed: 17029582]

Mombaerts P, Wang F, Dulac C, Chao SK, Nemes A, Mendelsohn M, Edmondson J, Axel R. Visualizing an olfactory sensory map. Cell. 1996; 87:675–686. [PubMed: 8929536]

Nikolaev A, Leung KM, Odermatt B, Lagnado L. Synaptic mechanisms of adaptation and sensitization in the retina. Nat Neurosci. 2013; 16:934–941. [PubMed: 23685718]

Ohmomo H, Ina A, Yoshida S, Shutoh F, Ueda S, Hisano S. Postnatal changes in expression of vesicular glutamate transporters in the main olfactory bulb of the rat. Neuroscience. 2009; 160:419–426. [PubMed: 19264112]

Ohshiro T, Angelaki DE, DeAngelis GC. A normalization model of multisensory integration. Nat Neurosci. 2011; 14:775–782. [PubMed: 21552274]

Olsen SR, Wilson RI. Lateral presynaptic inhibition mediates gain control in an olfactory circuit. Nature. 2008; 452:956–960. [PubMed: 18344978]

Olsen SR, Bhandawat V, Wilson RI. Divisive normalization in olfactory population codes. Neuron. 2010; 66:287–299. [PubMed: 20435004]

Oyibo HK, Znamenskiy P, Oviedo HV, Enquist LW, Zador AM. Long-term Cre-mediated retrograde tagging of neurons using a novel recombinant pseudorabies virus. Front Neuroanat. 2014; 8:86. [PubMed: 25232307]

Pinching AJ, Powell TP. The neuron types of the glomerular layer of the olfactory bulb. J Cell Sci. 1971; 9:305–345. [PubMed: 4108056]

Robinson BL, McAlpine D. Gain control mechanisms in the auditory pathway. Curr Opin Neurobiol. 2009; 19:402–407. [PubMed: 19665367]

De Saint Jan D, Hirnet D, Westbrook GL, Charpak S. External tufted cells drive the output of olfactory bulb glomeruli. J Neurosci. 2009; 29:2043–2052. [PubMed: 19228958]

Schoppa NE, Westbrook GL. AMPA autoreceptors drive correlated spiking in olfactory bulb glomeruli. Nat Neurosci. 2002; 5:1194–1202. [PubMed: 12379859]

Shepherd GM. Synaptic organization of the mammalian olfactory bulb. Physiol Rev. 1972; 52:864–917. [PubMed: 4343762]

Soucy ER, Albeanu DF, Fantana AL, Murthy VN, Meister M. Precision and diversity in an odor map on the olfactory bulb. Nat Neurosci. 2009; 12:210–220. [PubMed: 19151709]

Spors H, Wachowiak M, Cohen LB, Friedrich RW. Temporal dynamics and latency patterns of receptor neuron input to the olfactory bulb. J Neurosci. 2006; 26:1247–1259. [PubMed: 16436612]

Spors H, Albeanu DF, Murthy VN, Rinberg D, Uchida N, Wachowiak M, Friedrich RW. Illuminating vertebrate olfactory processing. J Neurosci. 2012; 32:14102–14108. [PubMed: 23055479]

Stopfer M, Jayaraman V, Laurent G. Intensity versus identity coding in an olfactory system. Neuron. 2003; 39:991–1004. [PubMed: 12971898]

Tatti R, Bhaukaurally K, Gschwend O, Seal RP, Edwards RH, Rodriguez I, Carleton A. A population of glomerular glutamatergic neurons controls sensory information transfer in the mouse olfactory bulb. Nat Commun. 2014; 5:3791. [PubMed: 24804702]

Vickers NJ. Mechanisms of animal navigation in odor plumes. Biol Bull. 2000; 198:203–212. [PubMed: 10786941]

Vinje WE, Gallant JL. Sparse coding and decorrelation in primary visual cortex during natural vision. Science. 2000; 287:1273–1276. [PubMed: 10678835]

Wachowiak M, Economo MN, Díaz-Quesada M, Brunert D, Wesson DW, White JA, Rothermel M. Optical dissection of odor information processing in vivo using GCaMPs expressed in specified cell types of the olfactory bulb. J Neurosci. 2013; 33:5285–5300. [PubMed: 23516293]

Whitesell JD, Sorensen KA, Jarvie BC, Hentges ST, Schoppa NE. Interglomerular lateral inhibition targeted on external tufted cells in the olfactory bulb. J Neurosci. 2013; 33:1552–1563. [PubMed: 23345229]

Willmore B, Tolhurst DJ. Characterizing the sparseness of neural codes. Network. 2001; 12:255–270. [PubMed: 11563529]

Wilson RI. Early olfactory processing in Drosophila: mechanisms and principles. Annu Rev Neurosci. 2013; 36:217–241. [PubMed: 23841839]

Wilson RI, Mainen ZF. Early events in olfactory processing. Annu Rev Neurosci. 2006; 29:163–201. [PubMed: 16776583]

Yaksi E, Wilson RI. Electrical coupling between olfactory glomeruli. Neuron. 2010; 67:1034–1047. [PubMed: 20869599]

Zhu P, Frank T, Friedrich RW. Equalization of odor representations by a network of electrically coupled inhibitory interneurons. Nat Neurosci. 2013; 16:1678–1686. [PubMed: 24077563]

Zhuang X, Masson J, Gingrich JA, Rayport S, Hen R. Targeted gene expression in dopamine and serotonin neurons of the mouse brain. J Neurosci Methods. 2005; 143:27–32. [PubMed: 15763133]

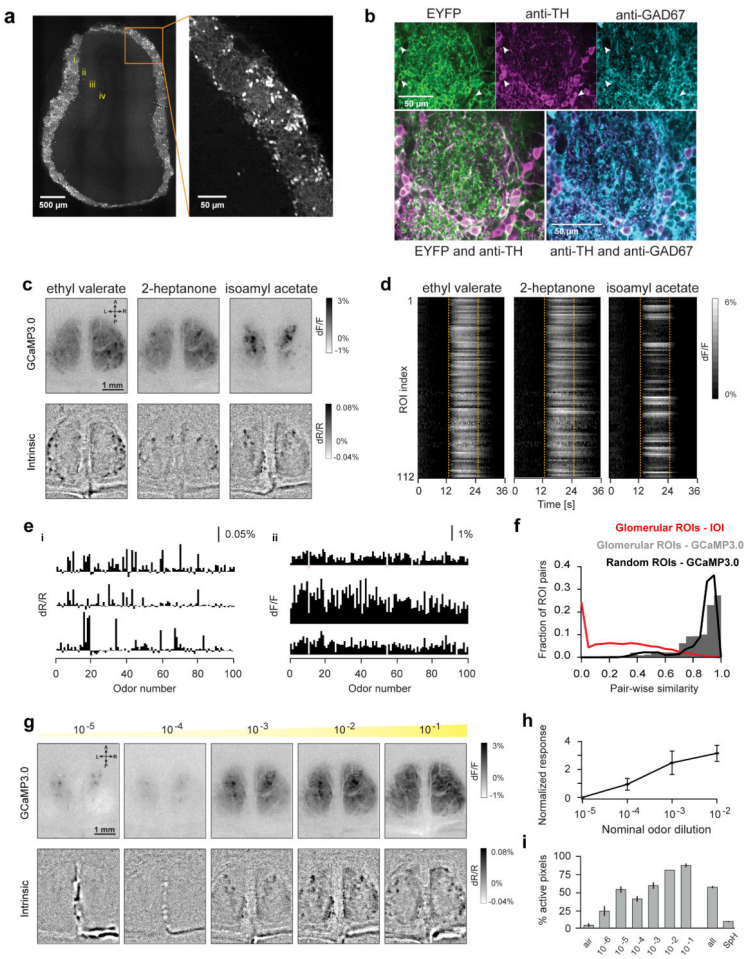

Figure 1. Long-range broadcast of odor inputs across the glomerular layer

A. Expression profile of a DAT-Cre x Ai9 reporter mouse line in a montage of two-photon images of an OB coronal slice. Inset shows DAT+ cells in the glomerular layer. i: glomerular layer; ii: External plexiform layer; iii: Mitral cell layer; iv: Granule cell layer.

B. *Top*, Confocal images from a DAT-Cre x Ai32 reporter mouse line, showing ChR2-EYFP fluorescence (*left*) and immunolabeling with TH antibody (*center*) and GAD67 antibody (*right*). Fiduciary marks show individual cell bodies. *Bottom left*, Pseudo-colored merge of ChR2-EYFP (green) and anti-TH (magenta). *Bottom right*, Pseudo-colored merge of anti-TH (magenta) and anti-GAD67 (cyan) staining.

C. Widefield GCaMP3.0 responses of DAT+ cells (*top*) and glomerular intrinsic optical imaging (IOI) signals (*bottom*) in response to Ethyl valerate, 2-heptanone and Isoamyl acetate in the same animal.

D. Time course of GCaMP3.0 signals of all 112 ROIs in response to the same odors from the example shown in **C**. ROIs were selected using glomerular outlines estimated from IOI. Dotted lines indicate odor presentation.

E. Odor response spectra (ORS) of three ROIs monitored via IOI (*i*) and GCaMP3.0 imaging (*ii*) to a panel of 100 odors. Rows correspond to different ROIs. Each bar shows the average normalized change in amplitude with respect to baseline (dF/F) for a given odor.

F. Distribution of ORS pairwise similarity for all ROI pairs within each hemi-bulb. Black line and gray bars respectively show similarity of ORS from IOI (14,211 pairs, 8 bulbs, 5 mice; average similarity 0.31±0.002) and GCaMP3.0 imaging (5,992 pairs, 3 bulbs, 3 mice; average similarity 0.83±0.002). ROIs were selected using glomerular outlines estimated from IOI. Red line shows distribution of pairwise similarity of GCaMP3.0 ORS for arbitrarily selected ROIs on the bulb surface (12,626 pairs, 5 bulbs, 3 mice; average similarity 0.88±0.001). Error values indicate standard error of the mean (SEM), unless explicitly stated otherwise.

G. GCaMP3.0 (*top*) and IOI (*bottom*) responses to increasing concentrations of Valeraldehyde in the same animal. Odor concentrations are reported as nominal dilutions in mineral oil (10^{-5}, 10^{-4}, 10^{-3}, 10^{-2}, 10^{-1}).

H. Average GCaMP3.0 responses with increasing odor concentrations. Each point represents the average response of all ROI-odor pairs (311 ROIs, 5 bulbs, 6 odors) normalized and subtracted from the corresponding individual responses at lowest odor concentration (10^{-5}).

I. Average spatial spread of GCaMP3.0 responses as a function of increasing odor concentration. Each bar shows average for all bulb-odor pairs (dilutions 10^{-5} to 10^{-2}: 5 bulbs, 6 odors; dilutions 10^{-6} and 10^{-1}: 2 bulbs, 6 odors). ‘Air’ corresponds to baseline response to clean air stimulation. ‘all’ corresponds to the pooled average spatial spread across all odors (10^{-2} dilution) in the data (285 bulb-odor pairs, 6 bulbs). SpH corresponds to the pooled average spatial spread across all odors and concentrations from widefield imaging of OMP-SpH mice (66 bulb-odor pairs, 2 bulbs).

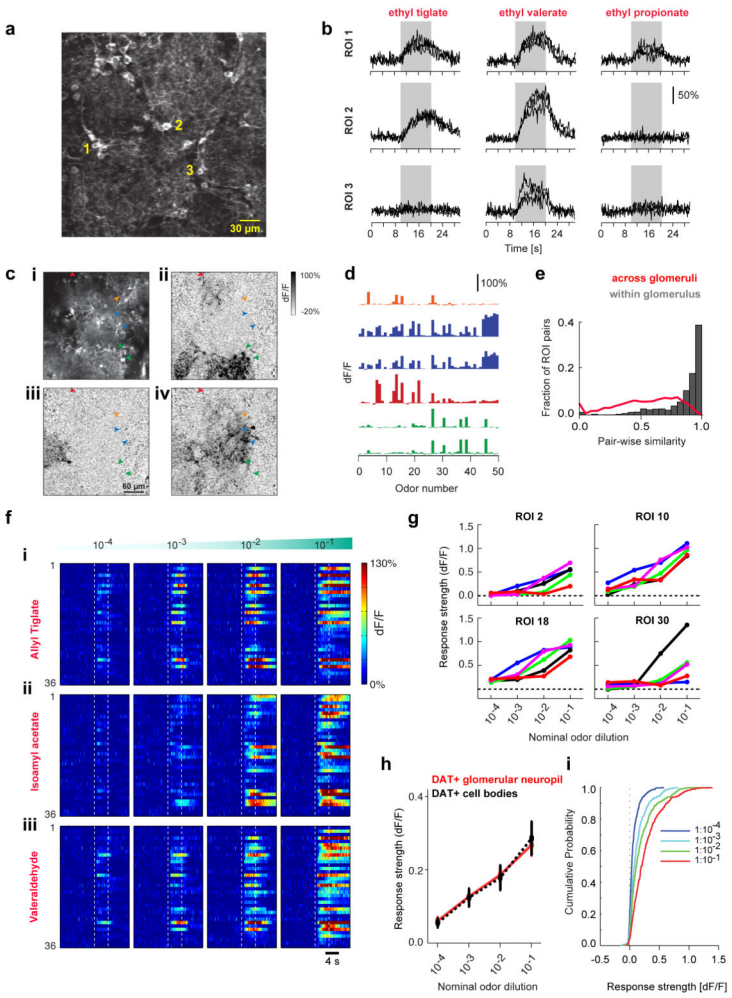

Figure 2. Responses of individual DAT+ cells are odor specific and scale with stimulus concentration

A. Two-photon image showing average resting fluorescence of a FOV from a DAT-Cre mouse x Ai38 reporter mouse line. Numbers denote representative DAT+ cell bodies.

B. GCaMP3.0 signals (dF/F) of DAT+ cells shown in **A** to Ethyl tiglate, Ethyl valerate and Ethyl propionate at 10^{-2} oil dilution. Black traces indicate individual trials. Gray band indicates odor presentation.

C. Two-photon images from a FOV showing average resting fluorescence (*i*) and odor evoked dF/F responses (*ii–iv*) of GCaMP3.0 labeled DAT+ cells around several glomeruli to 2,4,5-trimethyl thiazole (*ii*), 2-hexanone (*iii*) and Isobutyl propionate (*iv*). Fiduciary marks indicate cell bodies. Same color arrows indicate DAT+ cells selected around the boundaries of the same glomerulus.

D. Odor Response Spectra (ORS) of the DAT+ cells marked in **c** (*i*) to a panel of 50 odors. Colors indicate putative sister DAT+ cells.

E. Distribution of ORS similarity for all cell (ROI) pairs within individual FOVs. Gray bars and red line show similarity of ORS corresponding to DAT+ cell bodies selected around the

same glomeruli (1,390 pairs; average similarity 0.86±0.005) and randomly across (9,845 pairs; average similarity 0.56±0.003) glomeruli respectively. 331 ROIs, 50 odors, 4 mice.

F. GCaMP3.0 signals (dF/F) from 59 DAT+ cells to increasing concentrations of Isoamyl acetate, Valeraldehyde and Heptanal within the same FOV. Color indicates normalized change in fluorescence with respect to pre-odor baseline. Dotted lines mark odor presentation.

G. Mean odor response (5 repeats) of four example DAT+ cells in **F** to increasing concentrations of Allyl tiglate (blue), Isoamyl acetate (cyan), Valeraldehyde (green), Ethyl valerate (magenta) and Heptanal (red).

H. Mean of odor response from all glomerular ROIs selected (red) and for individual DAT+ cell bodies (dotted black) across five odors, at 4 different concentrations. 34 glomerular ROIs, 110 DAT+ cells in 3 mice.

I. Cumulative distribution of DAT+ cells' odor responses across 4 concentrations (n = 110 DAT+ cells, 3 mice).

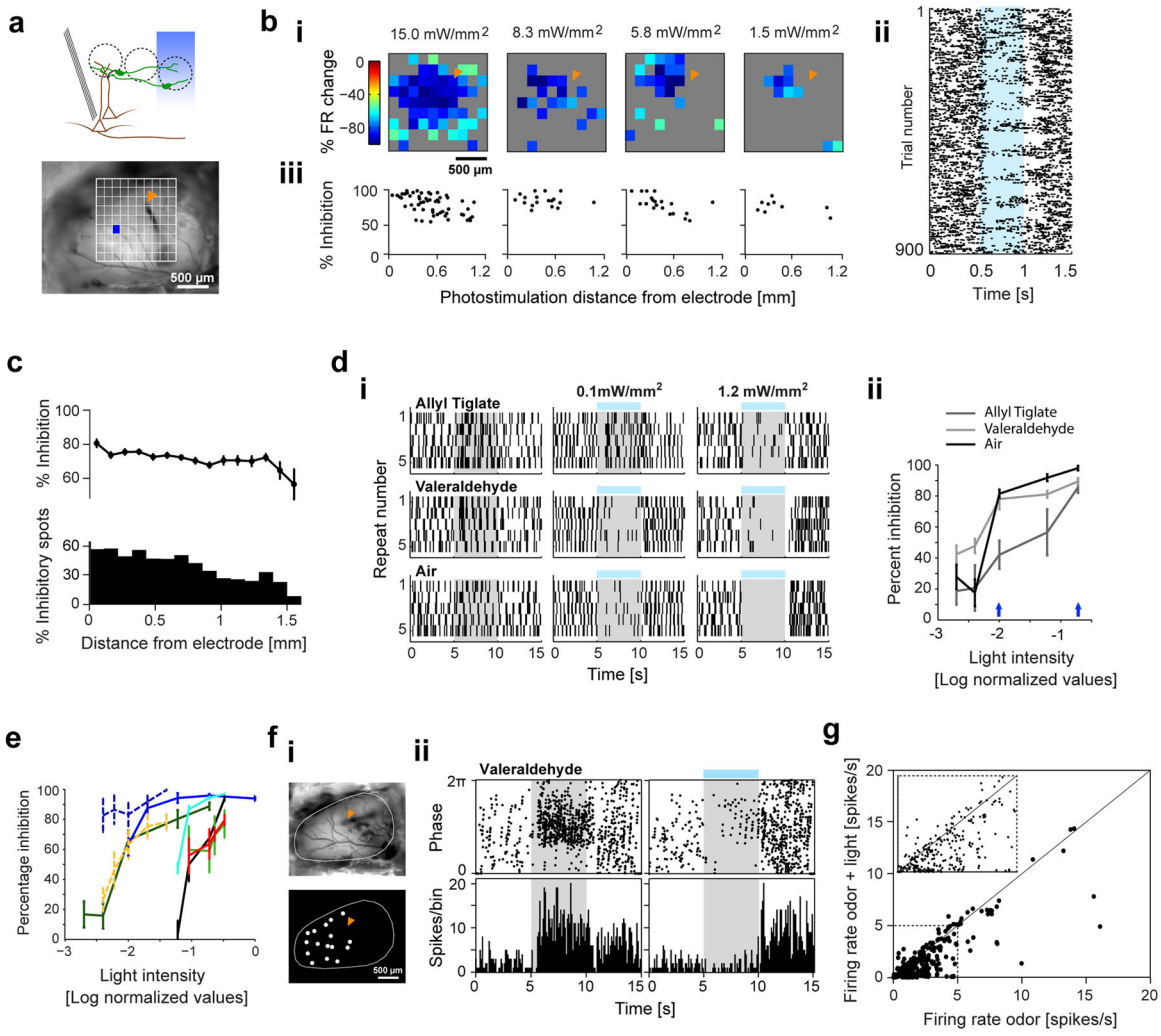

Figure 3. Photoactivating DAT+ cells results in long-range suppression of M/T cell firing

A. *Top*, Schematic of the experiment for optogenetic stimulation of ChR2-expressing DAT+ cells (green) with simultaneous M/T (brown) recordings. *Bottom*, Camera image of the OB, an example spot for photostimulation (130 µm × 130 µm) and fiduciary mark shows location of recording electrodes. Only spots that evoked a significant change from baseline are shown (two-sample t-test, $p < 0.05$).

B. (*i*) 2D light map of one M/T unit with blue light spots at four different light intensities (15, 8.3, 5.8, 1.5 mW/mm^2). Color indicates percentage change in M/T firing with respect to pre-light stimulation baseline (15 repeats). (*ii*) Spike raster showing individual trials from the light mapping session in (*i*) (15 mW/mm^2). Pixels, from *bottom left to top right corner*, in the light map are re-ordered as *top to bottom rows* in the spike raster. All repeats for each pixel are stacked together. Blue band indicates photostimulation. (*iii*) Strength of light-evoked inhibition as a function of photostimulation distance from the recording site, for the light maps in (*i*). Each dot represents percentage inhibition from baseline upon stimulation of an individual spot. Only spots that evoked a significant change from baseline are plotted (two-sample t-test, $p < 0.05$).

C. Strength of light-evoked inhibition (*top*) and fraction of significantly inhibited spots (*bottom*, two-sample t-test, $p < 0.05$) as a function of photostimulation distance from the recording site. Each dot/bar denotes average of all spots from 12 M/T units, 4 mice. Light intensity: 15 mW/mm^2.

D. *(i)* Spike rasters of an M/T unit upon presentation of Allyl tiglate (first row), Valeraldehyde (second row) and spontaneous activity (third row) by itself, or with full-field blue light stimulus at two different light intensities (second and third columns). Gray band indicates odor stimulus. Blue line indicates light stimulus. *(ii)* Percentage inhibition of firing rate $((FR_{odor} - FR_{odor+light})/FR_{odor})$ as a function of normalized blue light intensity plotted on log scale for the unit in *(i)*. Blue arrows denote the light intensities corresponding to rasters in *(i)*.

E. Summary of percentage inhibition versus blue light intensity. Each line denotes the average percentage inhibition across 5 odors for a single M/T unit (n = 8 units, 2 mice). Dotted lines represent M/T units recorded in one mouse and solid lines those recorded in a second mouse. Maximum light intensity was 7.9 mW/mm^2.

F. (*i*) Camera image of the OB (*top*) and light masks used for photoactivation (*bottom*) during the recording session shown in (*ii*). Fiduciary mark (orange) indicates location of recording electrodes. (*ii*) Peri-stimulus time histograms (PSTH, 500 ms bins) of an example M/T unit in response to 'Valeraldehyde' (dilution 10^{-3}) (*top*) and 'Valeraldehyde + blue light stimulation' (*bottom*). Gray band and blue line indicates odor and light stimulus respectively.

G. Scatter plot of average firing rates of individual M/T units during 'odor' and 'odor + light'. Points above and below the diagonal respectively denote excitation and inhibition of M/T firing. 351 cell-odor pairs, 41 M/T units from 6 mice.

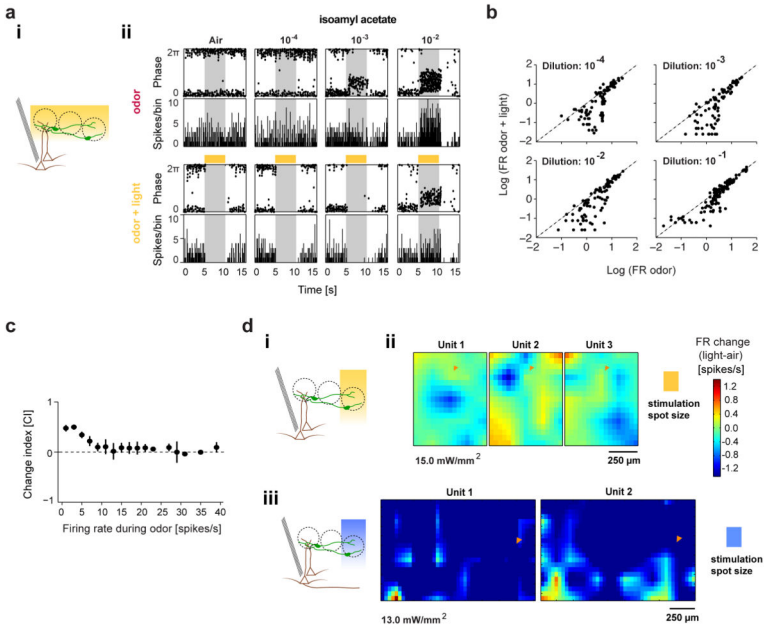

Figure 4. Optogenetic silencing of DAT+ cells suppresses M/T cells

A. (i) Schematic for *in vivo* full-field optogenetic inhibition of NpHR3.0-expressing DAT+ cells (green) with simultaneous M/T (brown) recordings. (ii) PSTH (500 ms bins) of an example M/T unit during baseline ('air') and increasing concentrations of Isoamyl acetate, in the absence ('odor') and presence ('odor + light') of DAT+ cell suppression (NpHR3.0 stimulation). Yellow bars indicate light stimulus.

B. Scatter plot of average firing rates of all recorded M/T units during 'odor' and 'odor + light' conditions, at four different odor concentrations. 10^{-4}: 110, 10^{-3}: 94, 10^{-2}: 110, 10^{-1}: 136 cell-odor pairs; 26 M/T units from 12 mice.

C. Summary plot showing average light-induced effect (change index, CI) for all cell-odor pairs (same as above) as a function of odor-evoked firing rate. CI is calculated as $[(FR_{odor} - FR_{odor+light})/(FR_{odor} + FR_{odor+light})]$ where $FR_{odor+light}$ and FR_{odor} correspond to the average odor-evoked firing in the presence and absence of light stimulation respectively. 450 cell-odor pairs, 26 M/T units, 12 mice.

D. *(i)* Schematics of optogenetic inhibition of NpHR3.0-expressing DAT+ cells (green) with simultaneous M/T (brown) recordings. *(ii)* 2D light maps of three simultaneously recorded M/T units upon optogenetic suppression of NpHR3.0 expressing DAT+ cells by yellow light (130 µm × 130 µm size, 500 ms, 50 repeats). Color denotes firing rate change (spikes/s) with respect to pre-light baseline. *(iii)* 2D light maps of two simultaneously recorded M/T units upon optogenetic activation of ChR2-expressing DAT+ cells by blue light (130 µm × 130 µm size, 500 ms, 15 repeats), plotted as in *(ii)*. Fiduciary mark shows location of recording electrodes.

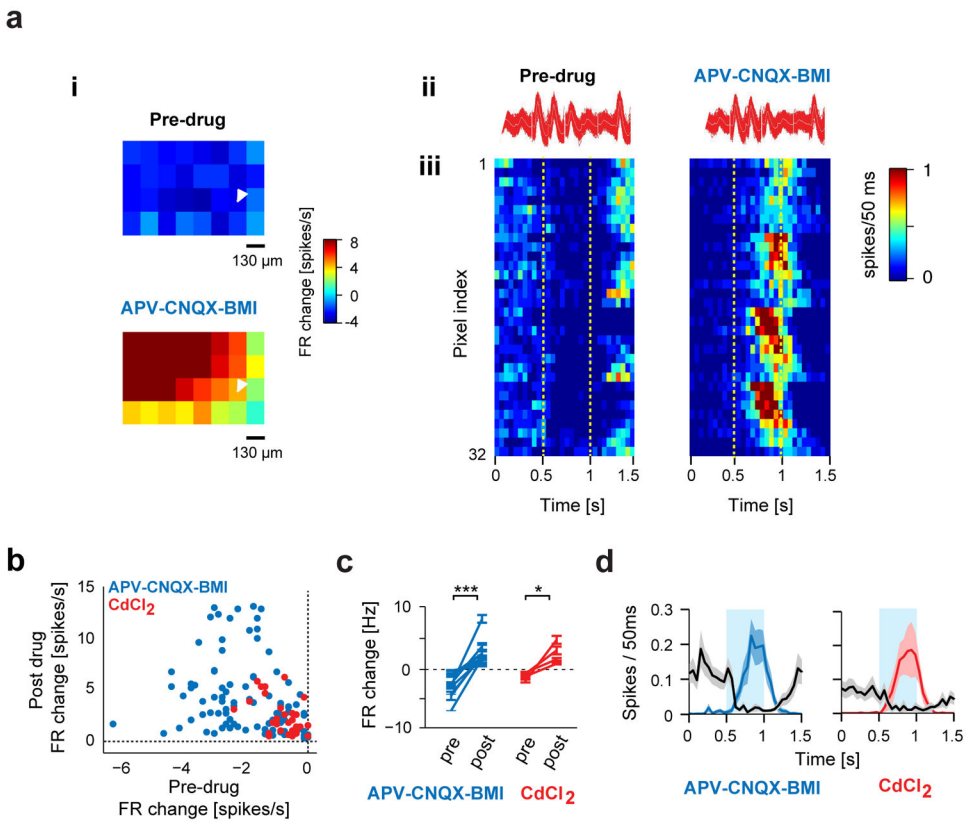

Figure 5. Light-induced suppression of M/T cells by DAT+ cells switches to excitation in presence of synaptic blockers

a. (*i*) Spike waveforms of an example M/T unit from a DAT-Cre mouse injected with DIO-ChR2-EYFP AAV virus before (*left*) and after (*right*) application of drugs. (*ii*) Example M/T unit shown in *(i)* showing change in firing upon mapping the OB surface with blue light spots (130 µm × 130 µm, 15 mW/mm^2, 15 repeats) before (*top*) and 30 min after (*bottom*) bath application of synaptic blockers (APV-CNQX-BMI). Color indicates percentage change in firing with respect to pre-light stimulation baseline. (*iii*) PSTHs of all spots from the light mapping session in (*i*), before (*left*) and after (*right*) drug application. Pixels, from *bottom left to top right corner*, in the light map are re-ordered as *top to bottom rows* in the PSTH. Dotted lines indicate light stimulus. Color indicates firing rate in each 50 ms bin. Fiduciary mark shows location of recording electrodes.

B. Scatter plot showing light-evoked change in firing rate of 15 M/T units during control and drug conditions. Each dot corresponds to a light stimulation spot that significantly modulated firing of the recorded M/T unit in the control condition. Blue and red dots correspond to APV-CNQX-BMI (92 spots, 11 M/T units) and $CdCl_2$ (32 spots, 4 M/T units) conditions respectively. Significance was tested using a paired t-test for all spots shown before and during drug application (blue dots, $p < 0.001$) and $CdCl_2$ (red dots, $p < 0.001$).

C. Summary plot showing light-evoked change in firing rate of all M/T units before and during APV-CNQX-BMI (blue, 11 M/T units, 4 bulbs) and $CdCl_2$ (red, 4 M/T units, 2 mice) application. * $p < 0.05$, *** $p < 0.001$, paired t-test.

D. Average time-course of firing rate of all recorded M/T units before (black) and during application of APV-CNQX-BMI (blue) or $CdCl_2$ (red). Only spots that significantly modulated the M/T firing rate in the control condition were included. Shaded bands indicate SEM across M/T units.

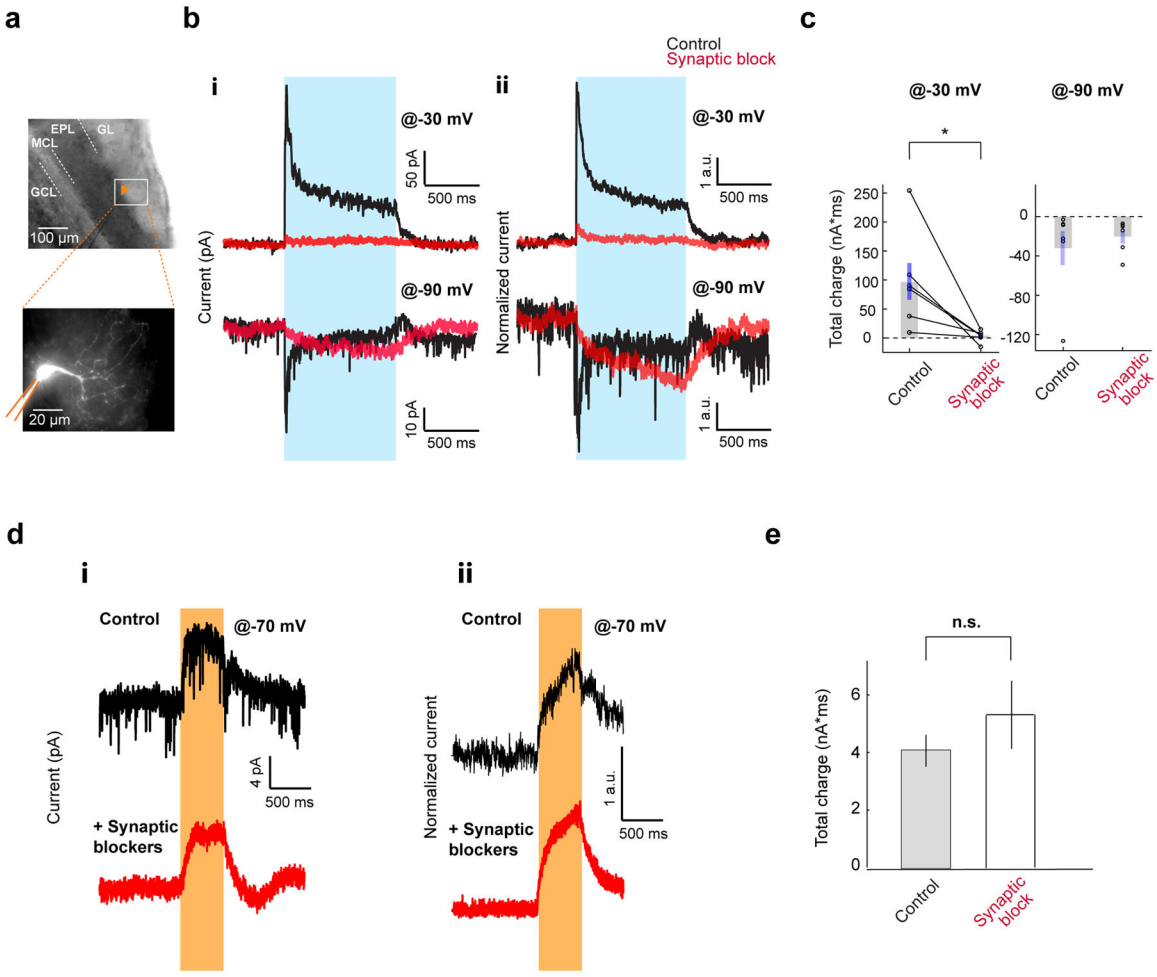

Figure 6. DAT+ cells interact with ET cells through both chemical and electrical synapses

A. Whole cell recordings from ET cells upon full-field activation of ChR2 expressing DAT+ cells in acute horizontal OB slices. *Top*, Image of the patch pipette (fiduciary mark) recording from an ET cell in the GL. *Bottom*, Typical morphology of an ET cell filled with Alexa 594 fluorescent dye.

B. Voltage clamp recordings from ET cells as above. (*i*) *Top*, Application of synaptic transmission blockers abolishes the light-induced outward current at −30 mV holding potential in a representative ET cell. Black and red traces (average of 10 repeats) represent trials pre- and post-drug application respectively. Blue bar indicates light stimulation. *Bottom*, in the same ET cell, the light-induced current reverses polarity at −90 mV holding potential (black trace, average of 10 repeats). Application of synaptic blockers (red trace, average of 10 repeats); (*ii*) Average of light-induced currents of 6 ET cells at −30 mV (*top*) and −90 mV (*bottom*) holding potentials, before (*black*) and after (*red*) pharmacological block of synaptic transmission. Currents from individual cells are normalized by the average current during the pre-drug light period.

C. Summary of total light-induced charge in ET cells shown in **B** before and after pharmacological block of synaptic transmission. Average light-induced total charge at −30 mV before (98±32 nA*ms) and after synaptic block (3.2±3.7 nA*ms) was significantly

different (n = 6 cells, p = 0.037, paired t-test). Average light induced total charge at −90 mV was −32±18 nA*ms and −20±6 nA*ms before and after synaptic block respectively (n = 6 cells).

D. Voltage clamp traces (−70 mV holding potential) from ET cells upon full-field inactivation of NpHR3.0 expressing DAT+ cells. *(i)* In an example ET cell, yellow light induces an outward current (*top*, average of 10 repeats), which persists in the presence of synaptic blockers (*bottom*, average of 10 repeats). *(ii)* Average light-induced currents across ET cells in the absence (*top*, n = 8) or in the presence of synaptic blockers (*bottom*, n = 12). Currents from individual cells are normalized by the average current during the light period.

E. Total light-induced charge at −70mV holding potential in the ET cells in the absence (4.1±0.55 nA*ms, n = 8 cells) and presence (5.3±1.2 nA*ms, n = 7 cells) of synaptic blockers (p = 0.37, two-sample unpaired t-test).

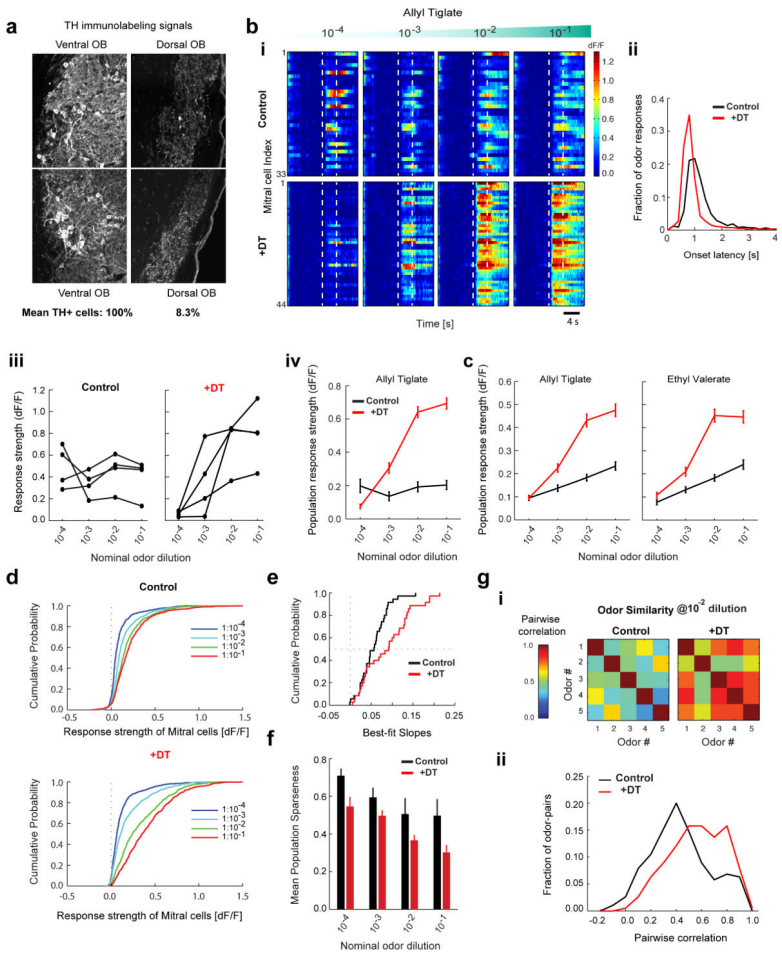

Figure 7. DAT+ cells implement gain control and decorrelate mitral cell odor responses

A. TH+ immunohistochemistry in the olfactory bulb of a DAT-Cre x Thy1-GCaMP3.0 mouse injected with AAV2.9-FLEX-DTR-GFP virus on the dorsal aspect of the OB followed by diphtheria toxin (DT) intraperitoneal injection. Confocal images of TH+ signal in two representative FOVs on the ventral (left) and dorsal (right) aspect of a given slice. Average counts of TH+ cells from all dorsal FOVs and from all ventral FOVs on in DTR injected mice, normalized by the number of visible glomeruli (100% for control and 8.3% for +DT, n = 1,259 cells, 8 FOVs, 2 mice). Residual signals mostly consisted of neuropil.

B. Baseline-subtracted, normalized GCaMP3.0 ensemble mitral cell responses to increasing concentrations of Allyl tiglate. *(Top)* DAY 0 before injection of DT (control, n = 33 cells). *(Bottom)* Different FOV in the same OB on DAY 7 after DT injection (+DT, n = 44 cells). Each row represents an individual mitral cell (ROI) in the same FOV. Color indicates (dF/F). Dotted lines indicate odor presentation (4 s).

C. *(i)* Distribution of onset latencies of mitral cell odor responses for control (1.55s ± 1.51s, n = 3660 cell-odor pairs) and +DT condition (1.2s ± 1.39s, n = 3000 cell-odor pairs). Numbers denote mean and standard deviation. Both the mean (two-sample t-test, $p < 10^{-18}$) and the variance (F-test, $p < 10^{-5}$) are significantly smaller in the +DT condition. ***(ii)*** Odor-evoked response (dF/F) of four example mitral cells from **B**, as a function of odor

concentration. ***(iii)*** Mean odor-evoked response (dF/F) of all mitral cells from **B** as a function of odor concentration for Allyl tiglate on DAY 0 (black, n = 33 cells) and DAY 7 after +DT administration (red, n = 44 cells).

D. Mean odor-evoked response (dF/F) of all mitral cells pooled across experiments as a function of odor concentration for Allyl tiglate and Ethyl valerate. Concentration response curves are shown for control (black, n = 168 cells, 7 FOVs, 7 mice) and +DT conditions (red, n = 150 cells, 7 FOVs, 3 mice).

E. Cumulative distribution of odor response strength of all mitral cells pooled across experiments, to five odors as a function of concentration in the control condition (n = 168 × 5 cell-odor pairs for each concentration) and after +DT injection (n = 150 × 5 cell-odor pairs for each concentration).

F. Cumulative distribution of slopes of the ensemble mitral cell concentration response curves separately fitted for each FOV and odor, in the control and +DT conditions (n = 35, 7 FOVs X 5 odors).

G. Population sparseness of mitral cell odor representations for each concentration in the control (black, n = 168 cells, 7 FOVs) and +DT conditions (red, n = 150 cells, 7 FOVs). Each bar denotes the mean population sparseness for 5 odors at each concentration.

H. *(i)* Matrix of correlation coefficients between the neural response spectra (length of vector = # of recorded neurons) for each odor pair at 1:100 dilution in the control and +DT conditions. *(ii)* Distribution of pairwise correlation coefficients between all stimulus pairs (n = 190 pairs, 5 odors at 4 concentrations) in the control and +DT conditions.

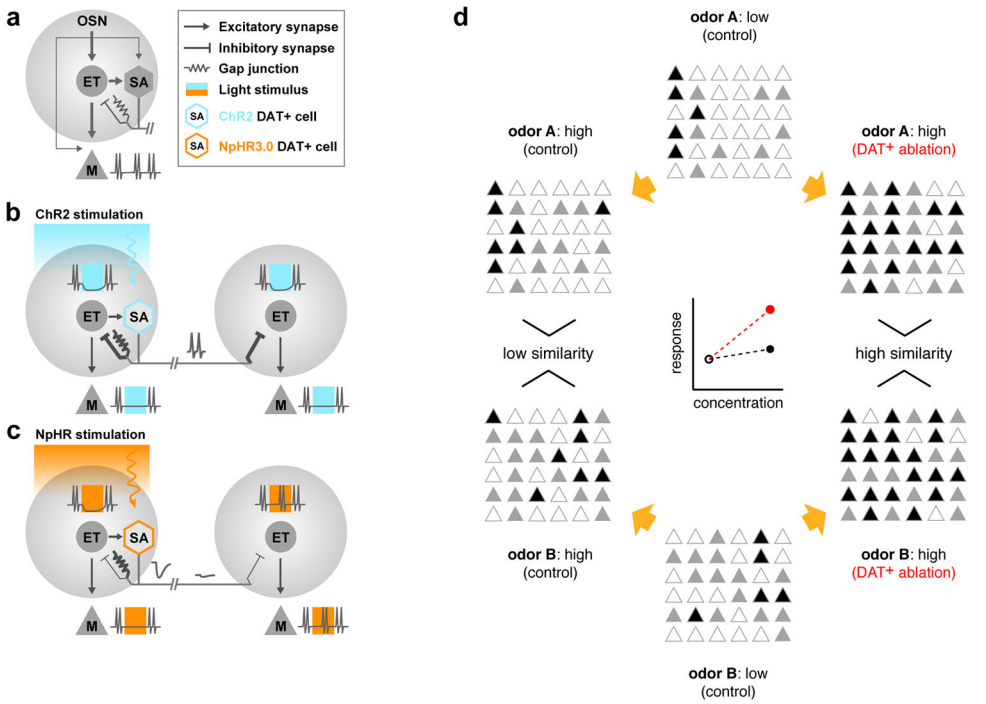

Figure 8. Schematic of the effect of DAT+ cell manipulations on M/T cell output

A. A simplified representation of the basic circuitry within a glomerulus. M/T cell and DAT + cell firing is primarily driven by excitatory inputs from ET cells, compared to relatively weak contribution of direct OSNs inputs. DAT+ cells form inhibitory synapses and gap-junctions onto ET cells.

B. Focal blue-light stimulation of ChR2-expressing DAT+ cells triggers synaptic inhibition of ET cells close by, as well as far away. Excitatory drive through gap-junctions is weak and readily outcompeted by the stronger synaptic inhibition, resulting in net inhibition of ET firing. Loss of excitatory ET drive consequently suppresses M/T cells.

C. Yellow-light stimulation of NpHR3.0-expressing DAT+ cells hyperpolarizes DAT+ cells and subsequently ET cells due to transmission of light-induced hyperpolarization across gap-junctions. The resultant ET inhibition translates into reduced M/T firing as observed in the extracellular recordings. In contrast to **B**, the observed inhibition is spatially restricted due attenuation via passive conductance. Note that both ChR2 and NpHR3.0 stimulation lead to net inhibition of ET cells, albeit via different mechanisms. Under both conditions, net inhibition of ET cells strongly suppresses M/T firing, thereby highlighting the central role played by ET cells in determining OB output.

D. At low concentrations, odors A and B activate distinct sets of M/T cells (middle). Higher concentrations increase both the number and amplitude of M/T responses (left). In the absence of DAT+ cells, more M/T cells are recruited (right) and the mean population activity increases more steeply with concentration (red). This results in increased overlap between the population representation of odors A and B. Concentration dependent lateral inhibition via DAT+ cells decreases the slope (gain) of the mean population activity of M/T

cells (black) and reduces overlap between population representations of odors A and B (decorrelation).